Journal of Hydrology: Regional Studies 66 (2026) 103635

Contents lists available at ScienceDirect

Journal of Hydrology: Regional Studies

journal homepage: www.elsevier.com/locate/ejrh

Rainfall and coastal water level relative timing as drivers of compound flooding in Haikou, China

Guofeng Wu [a,b], Hanqing Xu [a,b,*], Laixiang Sun [c,d], Can Lu [a,b], Hayley J. Fowler [e], Patrick Willems [f], Jun Wang [a,b,*], Qing Liu [a,b], Yue Sheng [a,b]

[a] Key Laboratory of Geographic Information Science (Ministry of Education), School of Geographic Sciences, East China Normal University, Shanghai 200241, PR China
[b] Institute for National Safety and Emergency Management, East China Normal University, Shanghai 200241, PR China
[c] Department of Geographical Sciences, University of Maryland, College Park, MD 20740, United States
[d] School of Finance & Management, SOAS University of London, London WC1H 0XG, United Kingdom
[e] School of Engineering and Tyndall Centre for Climate Change Research, Newcastle University, Newcastle upon Tyne, United Kingdom
[f] Hydraulics and Geotechnics Division, Department of Civil Engineering, KU Leuven, Leuven, Belgium

ARTICLE INFO

Keywords:
Compound flooding
Time-lag scenarios
Combined effect
Delft3D FM
Hydrodynamic modeling

ABSTRACT

Study Region: Urban area of Haikou, Hainan Province, China.
Study focus: Compound flooding in typhoon-prone coastal cities arises from the interaction between coastal water level and rainfall, but the role of their relative timing remains underexplored. This study proposes a framework that captures the relative timing for improved compound flooding assessment. Using the D-Flow FM model, we simulate 49 time-lag scenarios to quantify how timing (Δt) between coastal total water level and rainfall modulate inundation. For each scenario, we evaluate inundation volume and compute absolute (ΔM) and relative (ΔR) increments relative to the baseline. We delineate compound zones and decompose contributions from water level, rainfall, and their interaction.
New hydrological insights for the region: The results indicate that time-lags strongly shape compound flooding and produce nonlinear responses. Inundation is consistently larger when rainfall peaks before the coastal water level peak. A window from −19 h to −4 h yields volumes exceeding the historical event, and the maximum inundation occurs at −13 h with $\Delta R = 9.44\%$ and ($\Delta M = 8.53$ million m^3). Water level is the dominant driver, yet within compound zones, the interaction term exceeds rainfall alone. These findings highlight that taking $\Delta t = 0$ h as the worst-case can underestimate risks, emphasizing that the relative timing of rainfall and coastal water levels is a critical factor for managing compound flooding in coastal cities.

1. Introduction

Since the 1950s, global climate change has intensified the frequency and severity of compound flooding in coastal areas (Seneviratne et al., 2021; Marsooli et al., 2019; Feng et al., 2023). In low-lying, typhoon-prone coasts, slow-moving, rain-laden typhoons often produce both elevated coastal water levels (storm tide/surge) and intense rainfall. Storm tide drives coastal flooding,

* Corresponding authors at: Key Laboratory of Geographic Information Science (Ministry of Education), School of Geographic Sciences, East China Normal University, Shanghai 200241, PR China
E-mail addresses: hqxu@chm.ecnu.edu.cn (H. Xu), jwang@geo.ecnu.edu.cn (J. Wang).

https://doi.org/10.1016/j.ejrh.2026.103635
Received 3 March 2026; Received in revised form 17 May 2026; Accepted 8 June 2026
Available online 13 June 2026

while heavy rainfall causes urban waterlogging. Their overlap in space and time creates nonlinear interactions that amplify flood hazards beyond single-driver events (Wahl et al., 2015; Jalili Pirani and Najafi, 2020). For example, Hurricane Harvey in 2017 brought record rainfall (1539 mm) and a 3-meter storm tide to Texas, resulting in more than 80 fatalities and over $125 billion in losses in the Houston area (Blake and Zelinksy, 2018; Valle-Levinson et al., 2020).

Ignoring interactions among flood drivers can lead to underestimation of compound flooding hazards (Bevacqua et al., 2019, 2020; Xu et al., 2022; Gao et al., 2023). These interactions occur not only in space but also in time. The timing between water level and rainfall peaks can significantly influence flood magnitude, producing an amplifying effect (Juárez et al., 2022; Santiago-Collazo et al., 2024; Xu et al., 2024). While typhoons typically generate both drivers, their peaks often do not coincide, creating a "time lag" (Juárez et al.,2022; Xu et al., 2024). Many flood hazard assessments either assume synchronous peaks or treat flood drivers independently. So, the timing dynamics between flood drivers are not well captured (Zscheischler et al., 2018; Gori et al., 2020a, 2020b; Maymandi et al., 2022). This simplification can affect the accuracy of flood risk estimates, particularly in coastal areas exposed to extreme tropical cyclones. Understanding these interaction mechanisms is therefore essential for comprehensive flooding assessment in typhoon-prone coastal regions.

Hydrodynamic models offer a robust tool for examining the influence of time lags on compound flooding, as they dynamically simulate flood evolution under varying boundary conditions (Ming et al., 2022; Eilander et al., 2023; Shen et al., 2019; Wu et al., 2024). They are widely used to analyze inundation dynamics and disaster mechanisms (Gori et al., 2020a, 2020b; Juárez et al., 2022; Bao et al., 2024). Statistical models, by contrast, characterize the probabilistic nature of compound flooding (Zheng et al., 2013, 2014). Many studies emphasize the correlation and joint probability, but statistical models are generally limited in capturing the timing relationships between flood drivers (Phillips et al., 2022; Couasnon et al., 2020, 2022; Xu et al., 2023). In recent years, hydrodynamic studies have increasingly focused on the timing between rainfall and river discharge (storm surges) at the catchment scale, reflecting a well-recognized research trend (Hendry et al., 2019; Ye et al., 2021; Bilskie et al., 2021; Santiago-Collazo et al., 2024). Nevertheless, systematic research on how the relative timing between rainfall and coastal water level affects compound flooding outcomes remains limited in typhoon-prone coastal regions.

Hainan Province, China's largest special economic zone, is currently undergoing the strategic development of a free trade port. Haikou, the provincial capital, serves as the core city of Hainan Free Trade Port. Located along the main path of Northwest Pacific typhoons, Haikou ranks among the regions globally most threatened by extreme tropical cyclones (Zeng et al., 2022). Since 1949, Haikou has repeatedly experienced compound flooding during typhoons. Notable events include Typhoons Rammasun in 2014, Kalmaegi in 2014, and Capricorn in 2024, all of which caused substantial socioeconomic and property losses (Xu et al., 2019, 2025). During Typhoon Kalmaegi (TC1415), Haikou received 0.22 m of rainfall with a spring tide. The Xiuying gauge recorded a 2.09 m storm surge and a 4.52 m maximum water level—1.62 m above the warning level, a 100-year event (Shi et al., 2015; Liu et al., 2022).

Given the importance of time lags, this study proposes a risk assessment framework to quantify time-lag effects between coastal water level and rainfall using numerical hydrodynamic modeling. Based on hourly water level and rainfall data from TC1415 in Haikou, this study aims to: (1) construct time-lag scenarios based on a historical compound flood event, (2) simulate flood inundation under different time-lag conditions, (3) quantify the combined effects of time lags on inundation volume in compound flooding, and (4) evaluate the contributions of different flood drivers to compound flooding.

2. Materials

2.1. Study area

Haikou, located on the northern coast of Hainan Island (19°31' to 20°04' N, 110°07' to 110°42' E), features a topography with

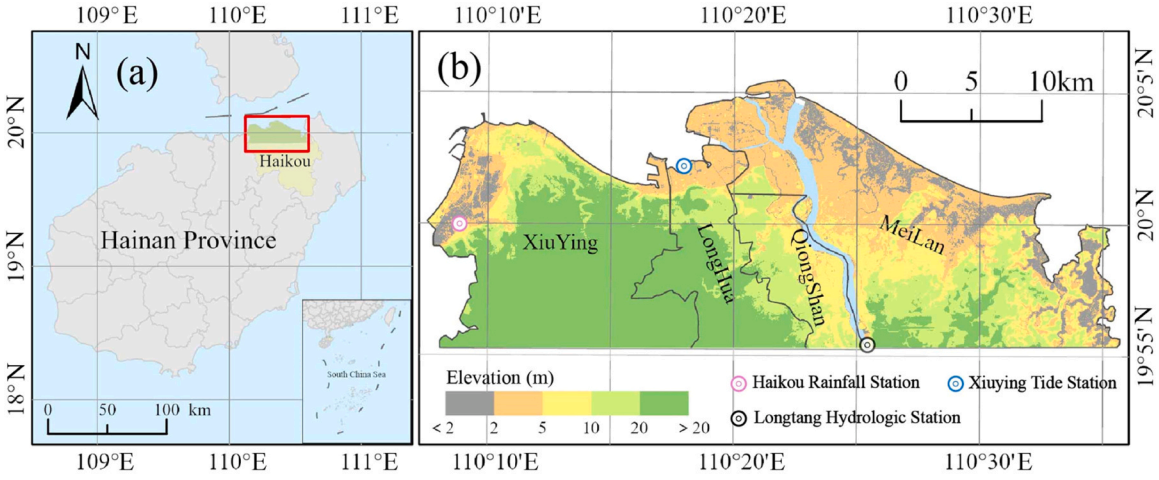

Fig. 1. Location map of the study area (a), digital elevation map of Haikou (b).

higher elevations in the northwest and southeast, and lower terrain along the Nandu River, with coastal plains to the north (Fig. 1). From 2015–2023, Haikou's urbanization rate surged from 55.09% to 83.34%, with the population exceeding 3 million by the end of 2023 (Haikou Bureau of Statistics, 2024. http://tjj.haikou.gov.cn/). Typhoons typically occur from July to October, with the region averaging 5.5 typhoons annually. These Typhoons often bring substantial water vapor, with the subtropical high-pressure system guiding them northward and westward, pushing seawater into the Qiongzhou Strait and triggering storm tide and heavy rainfall in the Haikou area (Zeng et al., 2022).

During TC1415 (September 15–17, 2014), Haikou experienced 0.22 m of accumulated rainfall, coinciding with an astronomical high tide. At the Xiuying Tide Station, a storm tide of 2.09 m was recorded, resulting in a total water level (TWL) of 4.52 m, which was 1.62 m above the local warning level of 2.90 m. This set a record for the highest water level since the station 's establishment. This compound flood event, characterized by both high water levels and heavy rainfall, impacted approximately 2.87 million people across Hainan Province and caused an estimated direct economic loss of 0.91 billion US dollars (https://www.chinanews.com.cn/gn/2014/09–22/6616378.shtml (Shi et al., 2015; Liu et al., 2022).

2.2. Dataset

Historical Typhoon Track and Hourly Grid Water Level Data: The typhoon track for TC1415 was extracted from the Historical Typhoon Track Dataset (1949–2019, 3-hourly resolution) provided by the Shanghai Typhoon Research Institute of the China Meteorological Administration. Using this track, Liu et al. (2022) integrated the Holland parametric typhoon model, the global tidal model (TPXO 8.0), and the D-Flow FM hydrodynamic model to generate high-resolution, hourly water-level simulations, which we adopted in this study.

Historical Rainfall: The hourly rainfall data during TC1415 were collected from the Haikou Rainfall Station (Fig. 1b) and are sourced from the China Meteorological Data Sharing Service Network (http://data.cma.cn/).

Topography Data: The 2018 Digital Elevation Model (DEM) of Haikou was provided by the Hainan Emergency Management Department, with a spatial resolution of 5 m, which had been interpolated to 30 m for this study. Bathymetric data for the South China Sea and the Beibu Gulf were obtained from the Global Bathymetric Chart of the Oceans (GEBCO), with a spatial resolution of 500 m (https://www.gebco.net/). Missing data were filled by averaging surrounding bathymetric values.

Discharge Data: The daily runoff data from 1960 to 2020 at the Longtang hydrologic station were provided by the Hainan Hydrology and Water Resources Survey Bureau.

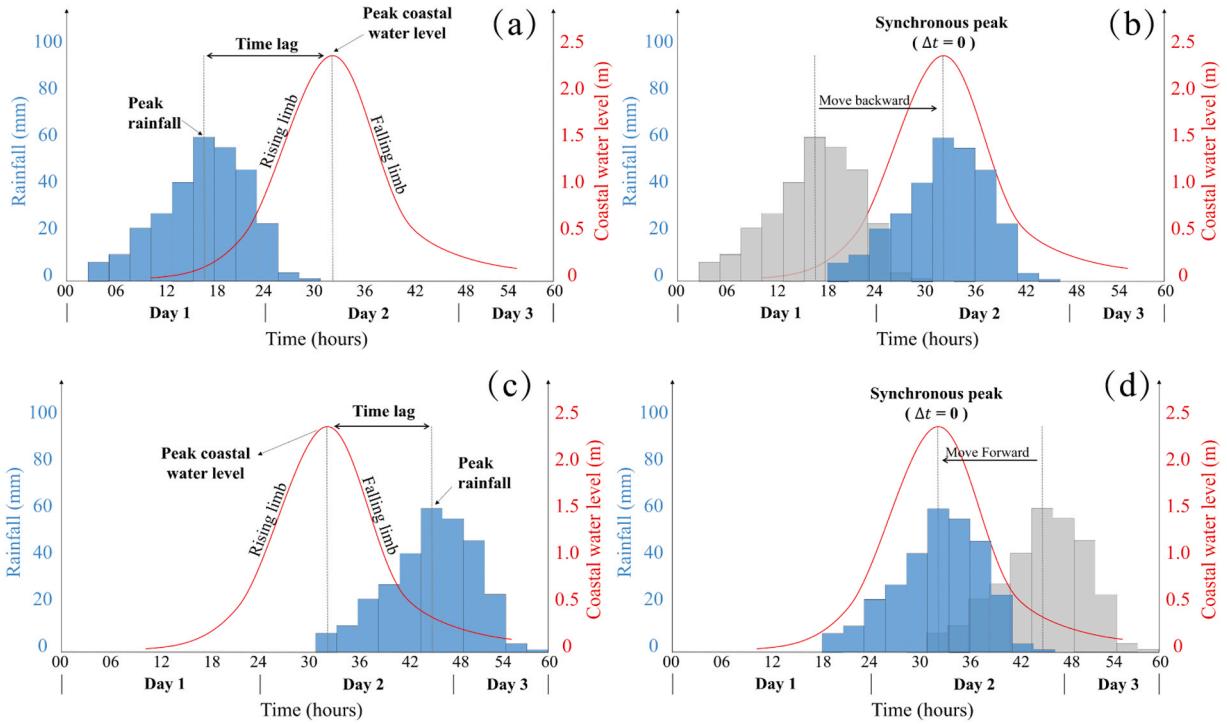

Fig. 2. Timing relationships between rainfall and water level peaks during compound flooding events. (a) Rainfall peak occurs before the water level peak; (b) Rainfall shifted backward to align with the water level peak (synchronous scenario); (c) Rainfall peak occurs after the water level peak; (d) Rainfall shifted forward to align with the water level peak (synchronous scenario).

3. Methods

3.1. Constructing time-lag scenarios between water-level and rainfall peaks for compound flooding

Fig. 2 illustrates the timing relationship of the considered flood drivers during compound flooding. We define Δt as the difference in timing between the rainfall peak and the coastal water level peak. When the rainfall peak occurs before the water level peak, Δt is negative; when it occurs after, Δt is positive; when $\Delta t = 0$, it indicates that the peaks are synchronous, with no time lag between them. To capture changes in inundation driven by the timing of flood drivers, we generated multiple time-lag scenarios by modifying the peak-time offset and using the resultant pairs as hydrodynamic simulation input boundaries. Scenario construction follows three steps: (1) determine the difference in timing between peak water level and peak rainfall (Δt); (2) shift the rainfall time series forward or backward along the timeline; and (3) construct combined boundary conditions of water level and rainfall for each time-lag scenario. In this study, we constructed 49 scenarios spanning $\Delta t \pm 24$ hours, to represent a range of potential compound flooding cases, and to evaluate the sensitivity of compound flood inundations to the timing of these peak drivers. The time-lag scenario uses $S_{\text{time lag}= \quad \Delta t}$ represent.

3.2. Hydrodynamic overland inundation modeling

D-Flow FM is widely used to simulate two-dimensional shallow water flow and surface runoff, making it suitable for modeling compound flooding processes (Lyddon et al., 2018; Huff et al., 2022). In this study, we constructed an overland inundation model for Haikou using the D-Flow FM and forced it at the coast with the water-level time series from the ocean model of Liu et al. (2022). The reconstruction was validated against observations at the Xiuying Tide Station (Fig. 1b), achieving RMSE = 0.14 m and $R^2 = 0.91$. Incorporating rainfall inputs and river discharge further enabled the simulation of compound-flood events across the region. The ocean model grid (Figure S1a) and the overland inundation model grid (Figure S1b) are provided in the Supporting Information.

The overland inundation model uses a hybrid mesh at ~30 m resolution: structured cells in riverine areas and unstructured triangular elements over inland regions, balancing computational efficiency and spatial fidelity (Figure S1 in Supporting Information). Roughness and infiltration parameters were derived from a 30 m land-use map, classified into residential, industrial, public buildings, transportation, agricultural, and green land (Liu et al., 2022). Based on runoff records from the Longtang Hydrologic Station on the Nandu River (1960–2020), we calculated a multi-year mean daily discharge of 165.81 m^3/s and applied this constant value at the upstream boundary to isolate the interactions between coastal water level and rainfall. Observed daily runoff at Longtang during TC1415 confirms that no significant upstream flood peak occurred (Figure S2 in Supporting Information). The rainfall boundary condition was based on hourly rainfall data during TC1415 collected from the Haikou Rainfall Station (Fig. 1b). This modeling framework underpins the simulation of compound inundation and the quantification of the time-lag effects.

3.3. Combined-effects calculation of time lags on compound flooding

Flood hazard is quantified by flood volume, calculated at the fixed peak flooding time as the domain-wide sum of depth-area products across all grid cells. For each time-lag scenario, the flood volume is calculated as follows: (1) identify the time step when the inundation extent reaches its maximum, (2) multiply inundation depth by pixel area for each grid cell, and (3) sum these values across all grid cells over the study domain.

To quantify the combined effects of time lags between coastal water level and rainfall, we used two indicators: the absolute increment (ΔM) and the relative increment (ΔR). Both are computed relative to a total-water-level (TWL) baseline (tide + surge) evaluated at the compound-peak time for each lag scenario. Throughout, "TWL-only baseline" refers to this reference, while "synchronous scenario ($\Delta t = 0$ h)" denotes the aligned-peaks compound case; the latter is not used for normalization. To avoid misleading normalizations where the TWL-only baseline inundation is near zero, a 0.05 m inundation threshold is applied. Relative metrics are reported only where the baseline depth meets this threshold. For each lag (Δt), the following procedure is implemented: (1) identify the compound peak time step (t^*); (2) compute the compound inundation volume V_{comp} (Δt, t^*); (3) extract the baseline inundation volume V_{base} (t^*) from the TWL-only baseline; (4) evaluate the combined effect using the following two indicators:

(i) Absolute increment (ΔM; units: million m^3):

$$\Delta M(\Delta t) = V_{comp}(\Delta t, t^*) - V_{base}(t^*) \quad (1)$$

(ii) Relative increment (ΔR; units: %):

$$\Delta R(\Delta t) = (V_{comp}(\Delta t, t^*) - V_{base}(t^*))/V_{base}(t^*) \times 100\% \quad (2)$$

Here, ΔR gives the percentage change in inundation volume of each time-lagged compound scenarios relative to the TWL-only baseline, and ΔM gives the corresponding absolute change.

3.4. Contribution of water level and rainfall in the time-lag scenarios

The influence of coastal water level and rainfall on compound flooding varies with their relative time lag. To quantify their contributions, we ran three simulations for each lag scenario: (1) TWL-only baseline, representing coastal flooding due to water level alone; (2) rainfall only, representing pluvial flooding due to rainfall alone; (3) combined water level and rainfall, representing the compound case. All simulations include a constant upstream river discharge to isolate the timing interaction between water level and rainfall. For each time-lag scenario, contributions are evaluated at the compound peak time t^*.

Let V_{wl} denote the inundation volume from the TWL-only run at t^*, V_r the volume from the rainfall alone runs at t^*, and $V_{compound}$ the volume from the compound runs at t^*. The fractional contributions of water level and rainfall are:

$$C_{wl} = \frac{V_{wl}}{V_{compound}} \times 100\% \tag{3}$$

$$C_r = \frac{V_r}{V_{compound}} \times 100\% \tag{4}$$

An interaction term captures the nonlinear contribution beyond the sum of individual drivers:

$$C_{other} = 1 - (C_{wl} + C_r) \tag{5}$$

Where C_{other} is the proportion of inundation volume attributable to interactions between water level and rainfall that are not explained by either driver alone.

To spatially identify regions where the two drivers interact, we delineated Compound Zones (*CA*) by comparing the compound flood map with the union of the TWL-only and rainfall-only maps for each lag scenario; *CA* consists of cells where compound inundation exceeds either single-driver inundation. For each time-lag scenario, we then quantified the contributions of water level (CA_{wl}), rainfall (CA_r), and their additional contribution (CA_{other}) within *CA* using the same formulas, with volumes restricted to the *CA* mask.

4. Results

4.1. Time-lag scenarios and hourly boundary conditions for compound flooding

Observational results reveal pronounced temporal asynchrony between water level and rainfall processes during TC1415 (Fig. 3a). The peak rainfall preceded the water level peak by 11 h. During TC1415, water levels began rising at 4:00 a.m. on September 16, 2014, reaching a peak of 4.28 m after 8 h (12:00 p.m.). Over the next 3 h, water levels rapidly decline, returning to normal by 3:00 p.m. The lowest water level, recorded at 8:00 p.m., was 0.67 m, resulting in a TWL fluctuation of 3.61 m. The rainfall pattern exhibited two distinct peaks, beginning at midnight on September 15. The first peak occurred 14 h later, at 1:00 p.m., with 31.38 mm of rainfall. The larger peak (41.17 mm) followed 25 h later at 1:00 a.m. on September 16. The observed peak mismatch phenomenon challenges the traditional synchronous peak assumption commonly used in compound flood simulations. As shown in Fig. 3b, whether the artificially aligned-peaks scenario (with the rainfall process shifted backward by 11 h) represents the worst-case flooding scenario requires further verification.

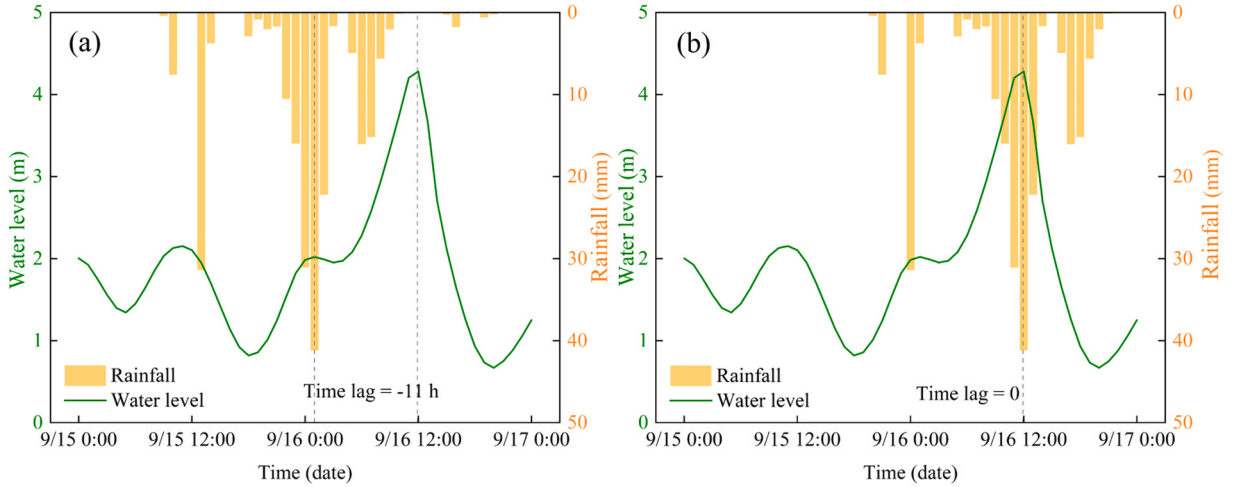

Fig. 3. The process curves of water level and rainfall are based on the TC1415 compound flood event at Haikou Rainfall Station and Xiuying Tide Station. (a) The process curves of water level and rainfall for the $\Delta t = -11$ h scenario; (b) the boundary conditions based on the synchronous peak scenario ($\Delta t = 0$ h).

4.2. Sensitivity of inundation maps to time lags between water level and rainfall

We ran the overland inundation model across multiple time-lag scenarios to assess inundation sensitivity. The synchronous scenario ($\Delta t = 0$ h) does not represent the worst-case scenario (Figure S3 in Supporting Information). Under $\Delta t = -11$ h scenario (TC1415), the inundation area is substantially larger than in the synchronous scenario (Fig. 4). Flooding primarily affects the northwestern urban region of Xiuying District, the northern coastal areas of Longhua District, the northern and northeastern coastal zones of Meilan District (Jiangdong New Area), as well as Xinbu and Haidian Island. And the low-lying inland areas also experience severe inundation (Fig. 4).

The maximum inundation volume occurs at $\Delta t = -13$ h (98.94 million m^3), with severe flooding along the coast, the Nandu River, and low-lying inland zones; depths exceed 0.5 m over large areas and surpass 3 m in the Jiangdong New Area (Figures 4d, S3). When rainfall peaks before the water level peak, inundation volumes are larger than when rainfall peaks afterward (Fig. 4b). As Δt became positive, overall inundation severity diminished. With sufficient delay, inland flooding nearly disappears, leaving coastal, TWL-only baseline scenario inundation as the dominant signal (Fig. 4a).

From $\Delta t = -24$–0 h, simulated volumes generally exceed both the ensemble mean (96.45 million m^3) and the synchronous case (98.02 million m^3), except at $\Delta t = -1$ h. When rainfall peak follows the water level peak ($\Delta t > 3$ h), volumes fall below both the ensemble mean and the synchronous case; by + 13 h, the volume is 95.33 million m^3 (3.61 million m^3 less than at −13 h), and by + 19 h, it reaches a minimum of 90.41 million m^3 (8.53 million m^3 less than at −13 h). After + 19 h, the compound volume converges toward the TWL-only baseline.

Within the −19 to −4 h window, all volumes exceed the historical TC1415 event (Fig. 4d). The maximum volume is 0.34 million m^3 higher than TC1415 and about 9 million m^3 above the TWL-only baseline. At $\Delta t = -16$ h, the volume is 98.93 million m^3 (0.33 million m^3 above TC1415; 8.52 million m^3 above TWL-only baseline). At $\Delta t = -6$ h, the volume is 98.90 million m^3 (0.30 million m^3 above TC1415; 8.49 million m^{3}above TWL-only). These results indicate that specific time lags can produce more severe inundation than both the historical event and the synchronous case.

4.3. Combined effects of time lag on inundation dynamics in compound flooding

We defined the absolute increment (ΔM) and relative increment (ΔR) of inundation volume relative to the baseline for each time-lag scenario to identify key lags and quantify combined effects. Overall, the time lag between peak water level and peak rainfall results in greater inundation than the baseline scenario (Fig. 5). During the period from −19 to −4 h, both ΔM and ΔR increase sharply, exceeding the baseline and the historical TC1415 value. Within this interval, ΔR exhibits a tri-modal pattern, with a maximum at −13 h; at this lag $\Delta M = 8.53$ million m^3 and $\Delta R = 9.44\%$, which is 0.71% higher than TC1415. At $\Delta t = -13$ h and −16 h, ΔR also remains high at 9.39% and 9.42%, respectively. Outside the −19 to −4 h window and within the 0–24 h, ΔR drops rapidly and remains near 0% after about 19 h; ΔM likewise approaches 0, indicating that the interaction between water level and rainfall has effectively

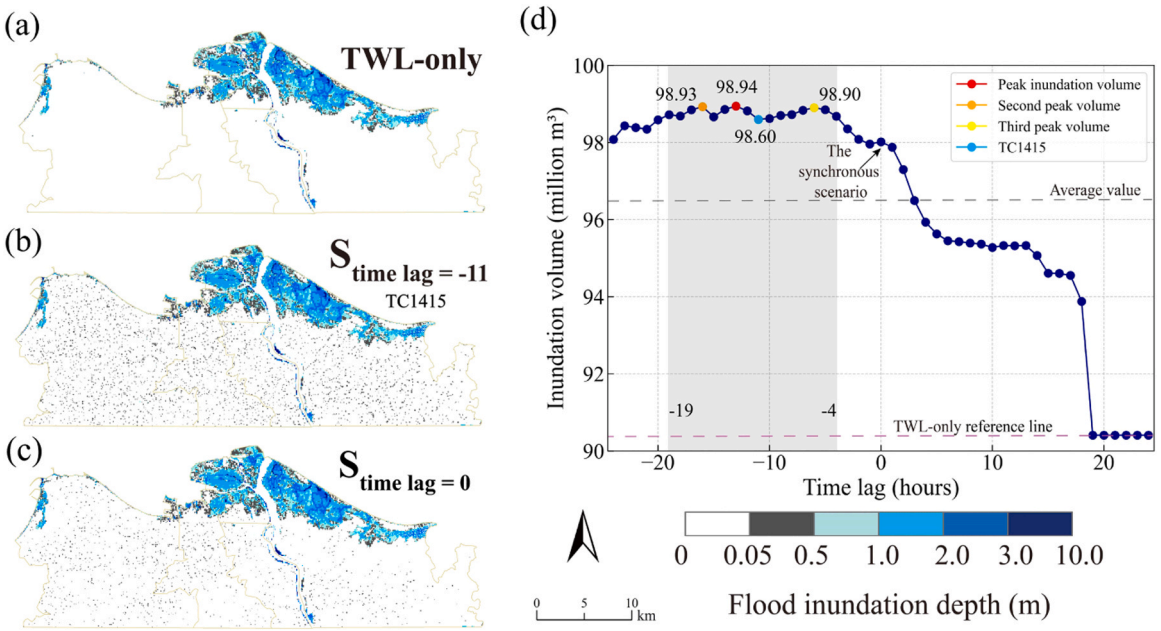

Fig. 4. Inundation maps at peak flooding for selected scenarios. (a) TWL-only baseline (no rainfall), (b) $\Delta t = -11$ h (TC1415), (c) $\Delta t = 0$ h (the synchronous scenario), and (d) inundation volumes for Δt from −24 to + 24 h. Red dots mark the location of the maximum inundation volume at $\Delta t = -13$ h.

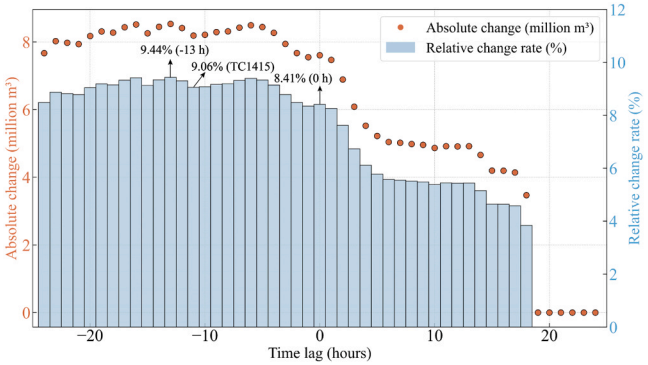

Fig. 5. Absolute and relative changes in inundation volume for each time-lag scenario relative to the TWL-only baseline (see Section 3.3). ΔM represents the absolute increment, and ΔR represents the relative increment.

ceased. The results reveal a nonlinear relationship between inundation volume and time lag, with absolute and relative changes not scaling proportionally with Δt.

Further analysis shows a clear asymmetry between positive and negative Δt. The mean ΔR for −24–0 h is 9.04%, while for + 1 to + 24 h it decreases to 4.22%. Notably, the actual TC1415 case yields $\Delta R = 9.06\%$, whereas the synchronous scenario ($\Delta t = 0$ h) yields $\Delta R = 8.41\%$. Thus, hazard assessments that assume peak synchronicity can underestimate extreme outcomes. Detailed ΔM and ΔR values for all scenarios are provided in Table S1 in the Supporting Information.

4.4. *Contribution of flood drivers across time-lag scenarios*

The relative time lag between water level and rainfall affects their contributions to compound flooding. As illustrated in Fig. 6, the water level is the dominant contributor, with its share increasing from −24 to 24 h (Fig. 6a). As the lag moves forward, the contribution rate stabilizes but exhibits nonlinear fluctuations. For $-24 \leq \Delta t \leq 0$, the mean C_{wl} is 91.71%, with a minimum of 91.38% at −13 h. Beyond 0 h, the mean rises to 96.02% and approaches 100% by 19 h. Rainfall shows the inverse pattern: For $-24 \leq \Delta t \leq 0$, the mean C_r is 5.65% (maximum 6% at −20 h), dropping to 4.77% at 0 h and to 0 after + 19 h. The interaction term C_{other} increases from −24 to + 18 h and then declines to ~0% after + 19 h. These trends suggest that as Δt becomes more positive, rainfall influence diminishes while the water level increasingly controls flooding; after + 19 h, the drivers effectively cease to interact. At $\Delta t = -13$ h (maximum inundation volume), neither water level nor rainfall alone attains its individual maximum, yet their combination exceeds both the baseline and the TC1415 record, evidencing a nonlinear response.

Within the compound-influenced area (*CA*), water level still accounted for the largest share. If the water level share is excluded, the remaining volume is partitioned as $CA_{other} = 61.1\%$ and $CA_r = 38.9\%$ (Fig. 6b). When rainfall peaks before water level ($\Delta t < 0$ h), the

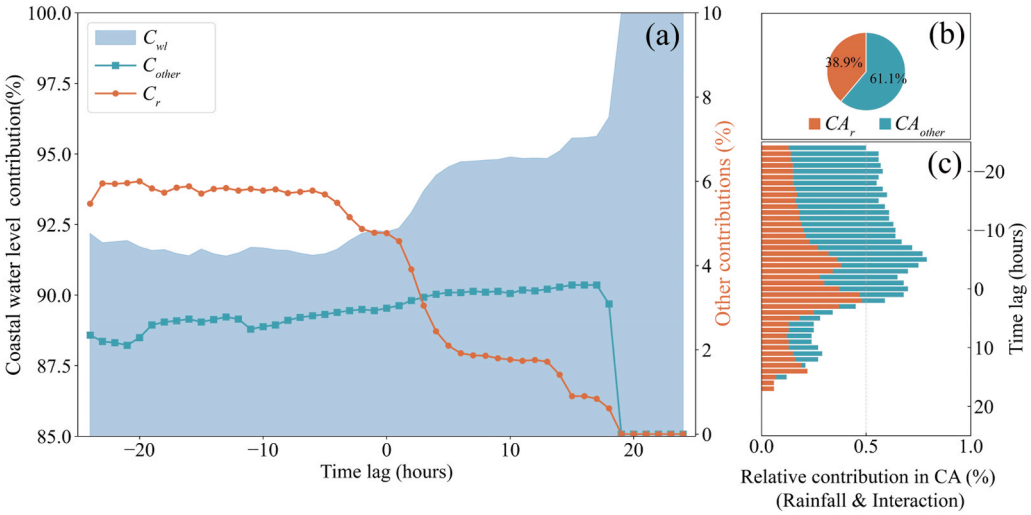

Fig. 6. Contribution rates of the flood drivers across time-lag scenarios. (a) Overall contributions of water level, rainfall, and interaction. The contribution of coastal water level is plotted on the left axis, while the contributions excluding water level (rainfall and interaction term) are plotted on the right axis. (b) Relative proportions of rainfall and interaction within *CA* after excluding the water level share. (c) Relative contribution of rainfall and interaction across time-lag scenarios in compound zones.

combined effect within *CA* is pronounced; throughout the −19 to −4 h window, $CA_{other} > CA_r$, with CA_{other} peaking near $\Delta t = -6$ to −7 h (Fig. 6c). This suggests interaction-driven amplification beyond the sum of individual contributions.

5. Discussion

5.1. Influence of time lag on compound flooding and flood management strategies

Unlike only rain-induced pluvial/fluvial or only water level-driven coastal flooding, typhoon-induced compound flooding is not a simple sum of these effects (Wahl et al., 2015; Bevacqua et al., 2019; Qiang et al., 2021). Our results reveal that the peaks of water level and rainfall occur at different times, and this time lag can amplify compound flooding. The TC1415 case ($\Delta t = -11$ h) demonstrates that assuming synchronous peaks ($\Delta t = 0$) as the worst-case condition underestimates flood risks. That the time lag between peaks strongly influences flood severity was also reported by Fang et al. (2021), Jiang et al. (2024) and You et al. (2024). But the compound effect resulting from the time lag between rainfall peaks and coastal water level peaks shows a threshold behavior. During the transition period (threshold window) between the two peaks (approximately −19 to −4 h), rainfall and coastal water levels interact in the convergence zone (the *CA*), producing a combined effect exceeding the sum of individual contributions ("1 +1 >2"). The low-gradient topography of the study area slows flood movement, and the limited river network extends inland flood response times, intensifying the interaction between rainfall and coastal water levels (Bao et al., 2024; Santiago-Collazo et al., 2024). We also noticed that a minor change in the threshold value used to calculate the inundation depth (e.g., 0.2 m) does not alter the overall pattern of flood inundation or the influence of the different time lag scenarios (Figure S4).

Rainfall-generated surface runoff requires time to reach the river, and water levels propagate upstream through tidal channels with a time lag (Gori et al., 2020a, 2020b). $\Delta t = -13$ h (2 h earlier than the TC1415) falls within the threshold window. Compared with $\Delta t \approx -19$ h, when the coastal water level has not yet risen significantly, and $\Delta t \approx -4$ h, when the coastal water level is close to its peak but the rate of rise is low. In this scenario ($\Delta t = -13$ h), rainfall had been ongoing for 17 h before reaching its peak and continued afterward without interruption, coinciding with a period of rapidly rising downstream water levels, which increased by more than 2 m (Figures S5). In the actual TC1415 event, the later rainfall peak allowed more time to drain compared with the −13 h scenario. As shown in Figure S6, intense inland rainfall had already saturated soils and river channels before the coastal water level peak. As a result, additional rainfall rapidly generates surface runoff rather than infiltrating, accelerating the volume of water reaching the *CA*. When rainfall reaches its peak (41.17 mm) and coincides with the rapidly rising coastal water level, water levels continue to rise for approximately 19 h until reaching the peak. The downstream water levels are elevated, reducing the water surface slope along the channel and obstructing upstream flow. When rainfall peaks closely before the water level rises, this blockage maximizes, producing the backwater effect that expands the inundation extent.

Under the dual pressures of climate change and rapid urbanization, traditional flood control measures that rely primarily on levees

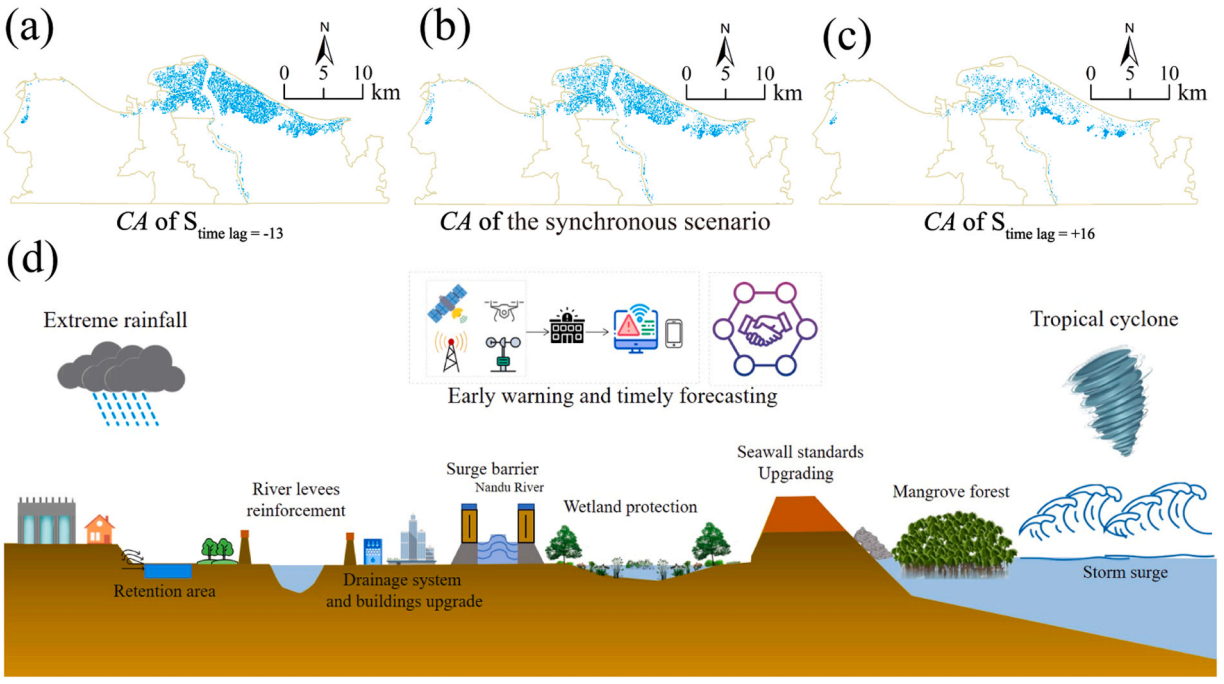

Fig. 7. Spatial interaction of compound flooding zones (*CA*) between rainfall-induced pluvial and coastal/fluvial flooding (a-c). Conceptual design of integrated structural and non-structural measures for compound flooding management in Haikou (d).

and other structural defenses face increasing challenges (Bubeck et al., 2016, 2017; Jongman, 2018; Wang et al., 2022). If peak impacts can be staggered in time, drainage and pumping systems have more time to respond, reducing the likelihood of severe flooding (Zhang et al., 2023; Chan et al., 2024). Hence, accurately identifying high-risk compound zones and issuing timely early warnings enables proactive resource deployment, lowering costs while improving emergency response efficiency (Moftakhari et al., 2017; Liu et al., 2024). Furthermore, when Δt does not fall within the −19 to −4 h window, the combined effect is markedly reduced. Fig. 7a-c show the spatial interaction of AC between rainfall-induced pluvial and coastal/fluvial flooding; the $\Delta t = -13$ h scenario exhibits the largest compound flooding zones.

Based on our findings regarding compound flooding in Haikou, we proposed a time-lag-informed flood management strategy that emphasizes peak-timing control to reduce compound flooding hazards (Fig. 7d). The core concept is to store floodwaters upstream, stagger discharge in the midstream, and release water downstream. To enhance temporary storage and buffer floodwaters, river levees should be strengthened, urban drainage systems upgraded, and the river network transformed to provide dynamic flood retention capacity. Underground storage tunnels can further attenuate surface runoff, introducing controlled delays in peak discharge. As the downstream section of the Nandu River, Haikou requires that levees along the river's estuary be raised to withstand flood depths of at least 3 m, corresponding to a 100–200-year return period. In coastal areas such as Haidian Island, Xinbu Island, and Jiangnan New District, a hybrid defense system that combines heightened seawalls with natural buffers (e.g., mangrove wetlands) can extend the dissipation process of storm tide energy and delay peak water levels (Jongman, 2018; Timmerman et al., 2021). In the main urban area along the Nandu River, levees on the left bank should be elevated to at least a 100-year return level, while those on the right bank should reach at least a 50-year return period. At the neighborhood scale, green roofs and rain gardens help intercept rainfall and reduce instantaneous runoff loads during critical periods (Wang et al., 2021; Cabana et al., 2023; Dharmarathne et al., 2024). Additionally, storm tide barriers at river mouths can block coastal floodwaters from entering urban areas, further mitigating compound flooding hazards (Orton et al., 2023). Due to climate change, sea level rise is expected to increase coastal water levels and may alter the timing and magnitude of compound flooding. By managing peak timing and integrating both structural and non-structural measures, these strategies can help enhancing Haikou's resilience to future compound flood events.

5.2. *Boundaries of the present study and future work*

This study identified key time-lag windows and spatial compound zones in Haikou City, providing a basis for targeted flood prevention. Although the study centers on a single TC1415, the methodological framework is generalizable. The findings reveal that the commonly used synchronized-peak assumption in compound flooding modeling does not necessarily represent the worst-case.

We focus on the timing between the coastal water level and rainfall. Other important lags in compound flooding systems—such as rainfall–runoff and rainfall–drainage response—also affect inundation because flood dynamics depend on both current and antecedent conditions, which vary in time and space (Wu et al., 2023; Daramola et al., 2025). The proposed risk-assessment framework can be transferred to other regions and drivers through a concise workflow: (1) select target drivers and construct lag scenarios using local data; (2) simulate compound events; (3) identify critical time windows and compound interaction zones; (4) use results to guide infrastructure upgrades and policy interventions.

Applicability to other typhoon-prone cities will depend on local hydrogeomorphology; critical lag thresholds are likely to differ with watershed scale, relief, storm characteristics, and coastal defenses. Climate change may further shift these thresholds, underscoring the need for continuous monitoring of lag patterns. Urban drainage capacity and soil moisture also modulate lag effects and should be incorporated in future research.

6. Conclusion

In this study, we simulated 49 time-lag scenarios using the D-Flow FM hydrodynamic model to examine how the relative timing between peak coastal water level and peak rainfall shapes compound flooding. The results show that time lag is a first-order control on inundation and that adopting the synchronous case ($\Delta t = 0$ h) as a proxy for the worst case can underestimate risk.

Flood volumes are systematically larger when rainfall peaks before the water level. A critical window from −19 to −4 h yields greater inundation than the historical TC1415 event, with a maximum at $\Delta t = -13$ h ($\Delta R = 9.44\%$; $\Delta M = 8.53$ million m^3). At this lag, severe flooding affects coastal areas, the Nandu River corridor, and low-lying inland zones, with depths > 0.5 m over large areas and > 3 m in the Jiangdong New Area.

Sensitivity analyses using absolute (ΔM) and relative (ΔR) metrics indicate a nonlinear response: changes in inundation do not scale proportionally with Δt. For positive lags, ΔR declines rapidly and approaches 0% after about + 19 h, indicating that timing interactions have effectively ceased and flooding is governed by coastal water level alone. Contribution analysis confirms that water level is the dominant driver; however, within compound zones, the interaction term exceeds rainfall alone ($CA_{\text{other}} = 61.1\%$; $CA_{\text{r}} = 38.9\%$), demonstrating a non-additive combined effect.

This study identified key time-lag windows and spatial compound zones relevant for practice. Management and adaptation should prioritize areas where drivers overlap in time and space and adopt time-lag-informed strategies—combining structural and nature-based measures, drainage upgrades, storage and pumping operations, and targeted early warning—to reduce compound-flood hazards under a changing climate.

CRediT authorship contribution statement

Guofeng Wu: Writing – review & editing, Writing – original draft, Visualization, Software, Methodology, Formal analysis, Data curation, Conceptualization. **Hanqing Xu:** Writing – review & editing, Writing – original draft, Methodology, Conceptualization. **Laixiang Sun:** Writing – review & editing, Methodology, Conceptualization. **Can Lu:** Validation, Methodology, Data curation. **Hayley J. Fowler:** Methodology, Conceptualization. **Patrick Willems:** Writing – review & editing, Conceptualization. **Jun Wang:** Writing – review & editing, Supervision, Methodology, Conceptualization. **Qing Liu:** Validation, Software. **Yue Sheng:** Writing – review & editing.

Declaration of Competing Interest

The authors declare that they have no known competing financial interests or personal relationships that could have appeared to influence the work reported in this paper.

Acknowledgments

The work was supported by the National Natural Science Foundation in China (Grant Nos 42401087). We also sincerely thank the East China Normal University (ECNU) Support Program for Global Research Visits for awarding us a grant.

Appendix A. Supporting information

Supplementary data associated with this article can be found in the online version at doi:10.1016/j.ejrh.2026.103635.

Data availability

Data will be made available on request.

References

Bao, D., Xue, Z.G., Warner, J.C., 2024. Quantifying compound and nonlinear effects of hurricane-induced flooding using a dynamically coupled hydrological-ocean model. e2023WR036455 Water Resour. Res. 60. https://doi.org/10.1029/2023WR036455.

Bevacqua, E., Maraun, D., Vousdoukas, M.I., Voukouvalas, E., Vrac, M., Mentaschi, L., Mann, M., 2019. Higher probability of compound flooding from rainfall and storm surge in Europe under anthropogenic climate change. Sci. Adv. 5 eaaw5531. https://doi.org/10.1126/sciadv.aaw5531.

Bevacqua, E., Vousdoukas, M.I., Zappa, G., Hodges, K., Shepherd, T.G., Maraun, D., Mentaschi, L., Feyen, L., 2020. More meteorological events that drive compound coastal flooding are projected under climate change. Commun. Earth Environ. 1, 47. https://doi.org/10.1038/s43247-020-00044-z.

Bilskie, M.V., Zhao, H., Resio, D., Atkinson, J., Cobell, Z., Hagen, S.C., 2021. Enhancing flood hazard assessments in coastal louisiana through coupled hydrologic and surge processes. Front. Water 3, 609231. https://doi.org/10.3389/frwa.2021.609231.

Blake, E.S., and Zelinksy, D.A., 2018. National Hurricane Center Tropical Cyclone Report: Hurricane Harvey (AL092017). National Hurricane Center. ⟨https://www.nhc.noaa.gov/data/tcr/AL092017_Harvey.pdf⟩.

Bubeck, P., Aerts, J.C.J.H., de Moel, H., Kreibich, H., 2016. Preface: flood-risk analysis and integrated management. Nat. Hazards Earth Syst. Sci. 16, 1005–1010. https://doi.org/10.5194/nhess-16-1005-2016.

Bubeck, P., Kreibich, H., Penning-Rowsell, E.C., Botzen, W.J.W., de Moel, H., Klijn, F., 2017. Explaining differences in flood management approaches in Europe and in the USA—a comparative analysis. J. Flood Risk Manag. 10, 436–445. https://doi.org/10.1111/jfr3.12151.

Cabana, D., Rölfer, L., Evadzi, P., Celliers, L., 2023. Enabling climate change adaptation in coastal systems: A systematic literature review. e2023EF003713 Earth's. Future 11. https://doi.org/10.1029/2023ef003713.

Chan, F.K.S., Lu, X., Li, J., Lai, Y., Luo, M., Chen, Y.D., Wang, D., Li, N., Chen, W.-Q., Zhu, Y.-G., Chan, H.K., 2024. Compound flood effects, challenges and solutions: Lessons toward climate-resilient Chinese coastal cities. Ocean. Coast. Manag. 249, 107015. https://doi.org/10.1016/j.ocecoaman.2023.107015.

Couasnon, A., Eilander, D., Muis, S., Veldkamp, T.I.E., Haigh, I.D., Wahl, T., Winsemius, H.C., Ward, P.J., 2020. Measuring compound flood potential from river discharge and storm surge extremes at the global scale. Nat. Hazard. Earth. Syst. 20, 489–504. https://doi.org/10.5194/nhess-20-489-2020.

Couasnon, A., Scussolini, P., Tran, T.V.T., Eilander, D., Muis, S., Wang, H., Nguyen, H.Q., Winsemius, H.C., Ward, P.J., 2022. A flood risk framework capturing the seasonality of and dependence between rainfall and sea levels—an application to Ho Chi Minh City, Vietnam. e2021WR030002 Water Resour. Res. 58. https://doi.org/10.1029/2021WR030002.

Daramola, S., Muñoz, D.F., Moftakhari, H., Moradkhani, H., 2025. A cluster-based temporal attention approach for predicting cyclone-induced compound flood dynamics. Environ. Modell. Softw. 191, 106499. https://doi.org/10.1016/j.envsoft.2025.106499.

Dharmarathne, G., Waduge, A.O., Bogahawaththa, M., Rathnayake, U., Meddage, D.P.P., 2024. Adapting cities to the surge: a comprehensive review of climate-induced urban flooding. Results Eng. 22, 102123. https://doi.org/10.1016/j.rineng.2024.102123.

Eilander, D., Couasnon, A., Leijnse, T., Ikeuchi, H., Yamazaki, D., Muis, S., Dullaart, J., Haag, A., Winsemius, H.C., Ward, P.J., 2023. A globally applicable framework for compound flood hazard modeling. Nat. Hazard. Earth. Syst. 23 (2), 823–846. https://doi.org/10.5194/nhess-23-823-2023.

Fang, J., Wahl, T., Fang, J., Sun, X., Kong, F., Liu, M., 2021. Compound flood potential from storm surge and heavy precipitation in coastal China: dependence, drivers, and impacts. Hydrol. Earth Syst. Sci. 25, 4403–4416. https://doi.org/10.5194/hess-25-4403-2021.

Feng, J., Li, D., Li, Y., Zhao, L., 2023. Analysis of compound floods from storm surge and extreme rainfall in China. J. Hydrol. 627, 130402. https://doi.org/10.1016/j.jhydrol.2023.130402.

Gao, L., Mei, J., Li, J., Zhang, W., Lai, C., 2023. Effect of intense rainfall and high riverine water level on compound flood hazards in a river-valley city: A case study of Yingde. China J. Hydrol. 625, 130044. https://doi.org/10.1016/j.jhydrol.2023.130044.

Gori, A., Lin, N., Smith, J., 2020a. Assessing compound flooding from landfalling tropical cyclones on the North Carolina coast. e2019WR026788 Water Resour. Res. 56. https://doi.org/10.1029/2019WR026788.

Gori, A., Lin, N., Xi, D., 2020b. Tropical cyclone compound flood hazard assessment: From investigating drivers to quantifying extreme water levels. e2020EF001660 Earth'S. Future 8. https://doi.org/10.1029/2020EF001660.

Hendry, A., Haigh, I.D., Nicholls, R.J., Winter, H., Neal, R., Wahl, T., Joly-Laugel, A., Darby, S.E., 2019. Assessing the characteristics and drivers of compound flooding events around the UK coast. Hydrol. Earth Syst. Sci. 23, 3117–3139. https://doi.org/10.5194/hess-23-3117-2019.
Huff, T.P., Feagin, R.A., Figlus, J., 2022. Delft3D as a tool for living shoreline design selection by coastal managers. Front. Built Environ. 8, 926662. https://doi.org/10.3389/fbuil.2022.926662.
Jalili Pirani, F., Najafi, M.R., 2020. Recent trends in individual and multivariate compound flood drivers in Canada's coasts. e2020WR027785 Water Resour. Res. 56. https://doi.org/10.1029/2020WR027785.
Jiang, S., Tarasova, L., Yu, G., Zscheischler, J., 2024. Compounding effects in flood drivers challenge estimates of extreme river floods. Sci. Adv. 10 eadl4005. https://doi.org/10.1126/sciadv.adl4005.
Jongman, B., 2018. Effective adaptation to rising flood risk. Nat. Commun. 9, 1986. https://doi.org/10.1038/s41467-018-04396-1.
Juárez, B., Stockton, S.A., Serafin, K.A., Valle-Levinson, A., 2022. Compound flooding in a subtropical estuary caused by Hurricane Irma 2017. e2022GL099360 Geophys. Res. Lett. 49 (18). https://doi.org/10.1029/2022GL099360.
Liu, Q., Xu, H., Wang, J., 2022. Assessing tropical cyclone compound flood risk using hydrodynamic modelling: A case study in Haikou City, China. Nat. Hazard. Earth. Syst. 22 (2), 665–675. https://doi.org/10.5194/nhess-22-665-2022.
Liu, Y., Zhang, T., Ding, Y., Kang, A., Lei, X., Li, J., 2024. Exploring the driving factors of compound flood severity in coastal cities: a comprehensive analytical approach. Hydrol. Earth Syst. Sci. 28, 5541–5555. https://doi.org/10.5194/hess-28-5541-2024.
Lyddon, C., Brown, J.M., Leonardi, N., Plater, A.J., 2018. Flood hazard assessment for a hyper-tidal estuary as a function of tide-surge-morphology interaction. Estuar. Coast. 41, 1565–1586. https://doi.org/10.1007/s12237-018-0384-9.
Marsooli, R., Lin, N., Emanuel, K., Feng, K.R., 2019. Climate change exacerbates hurricane flood hazards along US Atlantic and Gulf Coasts in spatially varying patterns. Nat. Commun. 10, 3785. https://doi.org/10.1038/s41467-019-11755-z.
Maymandi, N., Hummel, M.A., Zhang, Y., 2022. Compound coastal, fluvial, and pluvial flooding during historical hurricane events in the Sabine-Neches Estuary, Texas. e2022WR033144 Water Resour. Res. 58 (12). https://doi.org/10.1029/2022WR033144.
Ming, X., Liang, Q., Dawson, R., Xia, X., Hou, J., 2022. A quantitative multi-hazard risk assessment framework for compound flooding considering hazard interdependencies and interactions. J. Hydrol. 607, 127477. https://doi.org/10.1016/j.jhydrol.2022.127477.
Moftakhari, H.R., AghaKouchak, A., Sanders, B.F., Matthew, R.A., 2017. Cumulative hazard: The case of nuisance flooding. Earth'S. Future 5, 214–223. https://doi.org/10.1002/2016EF000494.
Orton, P., Ralston, D., van Prooijen, B., Secor, D., Ganju, N., Chen, Z., Fernald, S., Brooks, B., Marcell, K., 2023. Increased utilization of storm surge barriers: A research agenda on estuary impacts. e2022EF002991 Earth'S. Future 11. https://doi.org/10.1029/2022EF002991.
Phillips, R.C., Samadi, S., Hitchcock, D.B., Meadows, M.E., Wilson, C.A.M.E., 2022. The devil is in the tail dependence: An assessment of multivariate copula-based frameworks and dependence concepts for coastal compound flood dynamics. e2022EF002705 Earth'S. Future 10. https://doi.org/10.1029/2022EF002705.
Qiang, Y., He, J., Xiao, T., Lu, W., Li, J., Zhang, L., 2021. Coastal town flooding upon compound rainfall-wave overtopping-storm surge during extreme tropical cyclones in Hong Kong. J. Hydrol. Reg. Stud. 37, 100890. https://doi.org/10.1016/j.ejrh.2021.100890.
Santiago-Collazo, F.L., Bilskie, M.V., Bacopoulos, P., Hagen, S.C., 2024. Compound inundation modeling of a 1-D idealized coastal watershed using a reduced-physics approach. e2023WR035718 Water Resour. Res. 60. https://doi.org/10.1029/2023WR035718.
Seneviratne, S.I., Zhang, X., Adnan, M., Badi, W., Dereczynski, C., Di Luca, A., Ghosh, S., Iskandar, I., Kossin, J., Lewis, S., Otto, F., Pinto, I., Satoh, M., Vicente-Serrano, S.M., Wehner, M., Zhou, B., 2021. Weather and climate extreme events in a changing climate. In: Masson-Delmotte, V., Zhai, P., Pirani, A., Connors, S.L., Péan, C., Berger, S., Caud, N., Chen, Y., Goldfarb, L., Gomis, M.I., Huang, M., Leitzell, K., Lonnoy, E., Matthews, J.B.R., Maycock, T.K., Waterfield, T., Yelekçi, O., Yu, R., Zhou, B. (Eds.), The Physical Science Basis. Contribution of Working Group I to the Sixth Assessment Report of the Intergovernmental Panel on Climate Change. Cambridge University Press, Cambridge, United Kingdom, pp. 1513–1766. https://doi.org/10.1017/9781009157896.013 (and New York, NY, USA).
Shen, Y., Morsy, M.M., Huxley, C., Tahvildari, N., Goodall, J.L., 2019. Flood risk assessment and increased resilience for coastal urban watersheds under the combined impact of storm tide and heavy rainfall. J. Hydrol. 579, 124159. https://doi.org/10.1016/j.jhydrol.2019.124159.
Shi, H., Li, W., Lv, Y., Feng, Z., 2015. Comparative analysis of two severe storm surge of Hainan Province in 2014. Mar. Forecasts 32 (04), 75–82.
Timmerman, A., Haasnoot, M., Middelkoop, H., Bouma, T., McEvoy, S., 2021. Ecological consequences of sea level rise and flood protection strategies in shallow coastal systems: A quick-scan barcoding approach. Ocean. Coast. Manag. 210, 105674. https://doi.org/10.1016/j.ocecoaman.2021.105674.
Valle-Levinson, A., Olabarrieta, M., Heilman, L., 2020. Compound flooding in Houston-Galveston Bay during Hurricane Harvey. Sci. Total. Environ. 747, 141272. https://doi.org/10.1016/j.scitotenv.2020.141272.
Wahl, T., Jain, S., Bender, J., Meyers, S.D., Luther, M.E., 2015. Increasing risk of compound flooding from storm surge and rainfall for major US cities. Nat. Clim. Chang. 5, 1093–1097. https://doi.org/10.1038/nclimate2736.
Wang, L., Cui, S., Li, Y., Huang, H., Manandhar, B., Nitivattananon, V., Fang, X., Huang, W., 2022. A review of the flood management: from flood control to flood resilience. Heliyon 8, e11763. https://doi.org/10.1016/j.heliyon.2022.e11763.
Wang, X., Guo, Y., Ren, J., 2021. The coupling effect of flood discharge and storm surge on extreme flood stages: A case study in the Pearl River Delta, South China. Int. J. Disast. Risk Sc. 12, 1–15. https://doi.org/10.1007/s13753-021-00355-5.
Wu, G., Liu, Q., Xu, H., Wang, J., 2024. Modelling the combined impact of sea level rise, land subsidence, and tropical cyclones in compound flooding of coastal cities. Ocean. Coast. Manag. 252, 107107. https://doi.org/10.1016/j.ocecoaman.2024.107107.
Wu, J., Zhang, Q., Li, Y., Xu, C.-Y., Ye, X., 2023. Spatial-temporal variations of stage-area hysteretic relationships in large heterogeneous lake–floodplain systems. J. Hydrol. 620, 129507. https://doi.org/10.1016/j.jhydrol.2023.129507.
Xu, H., Ragno, E., Jonkman, S.N., Wang, J., Bricker, J.D., Tian, Z., Sun, L., 2024. Combining statistical and hydrodynamic models to assess compound flood hazards from rainfall and storm surge: a case study of Shanghai. Hydrol. Earth Syst. Sci. 28, 3919–3930. https://doi.org/10.5194/hess-28-3919-2024.
Xu, H., Ragno, E., Tan, J., Antonini, A., Bricker, J.D., Jonkman, S.N., Liu, Q., Wang, J., 2023. Perspectives on compound flooding in Chinese estuary regions. Int. J. Disast. Risk Sc. 14, 269–279. https://doi.org/10.1007/s13753-023-00482-1.
Xu, H., Tian, Z., Sun, L., Ye, Q., Ragno, E., Bricker, J., Mao, G., Tan, J., Wang, J., Ke, Q., Wang, S., Toumi, R., 2022. Compound flood impact of water level and rainfall during tropical cyclone periods in a coastal city: the case of Shanghai. Nat. Hazard. Earth. Syst. 22, 2347–2358. https://doi.org/10.5194/nhess-22-2347-2022.
Xu, K., Wen, N., Zhuang, Y., 2025. Experimental research on the jacking effect of compound flooding in a coastal city: case study in the Meishe River basin, Haikou City. Advances in Water. Science 36 (03), 527–535.
Xu, H., Xu, K., Lian, J., Ma, C., 2019. Compound effects of rainfall and storm tides on coastal flooding risk. Stoch. Environ. Res. Risk Assess. 33, 1249–1261. https://doi.org/10.1007/s00477-019-01695-x.
Ye, F., Huang, W., Zhang, Y.J., Moghimi, S., Myers, E., Pe'eri, S., Yu, H.-C., 2021. A cross-scale study for compound flooding processes during Hurricane Florence. Nat. Hazard. Earth. Syst. 21, 1703–1719. https://doi.org/10.5194/nhess-21-1703-2021.
You, J.W., Wang, S., Zhang, B.E., 2024. Spatially seamless and temporally continuous assessment on compound flood risk in Hong Kong. J. Hydrol. 645, 132217. https://doi.org/10.1016/j.jhydrol.2024.132217.
Zeng, P., Su, Z., Fang, W., Zhang, H., Yu, L., 2022. Typhoon flooding loss assessment in haikou city based on high precision building type data. J. Catastro 37, 155–165.
Zhang, Z., Lu, Y., Hu, D., Guo, F., Yu, Z.Y., Song, Z.Y., Chen, P., Wu, J.X., Huang, W.P., 2023. A cross-scale modeling framework for simulating typhoon-induced compound floods and assessing the emergency response in urban regions. Ocean. Coast. Manag. 245, 106863. https://doi.org/10.1016/j.ocecoaman.2023.106863.
Zheng, F., Westra, S., Sisson, S.A., 2013. Quantifying the dependence between extreme rainfall and storm surge in the coastal zone. J. Hydrol. 505, 172–187. https://doi.org/10.1016/j.jhydrol.2013.09.054.

Zheng, F., Westra, S., Leonard, M., Sisson, S.A., 2014. Modeling dependence between extreme rainfall and storm surge to estimate coastal flooding risk. Water Resour. Res. 50, 2050–2071. https://doi.org/10.1002/2013WR014616.

Zscheischler, J., Westra, S., van den Hurk, B.J.J.M., Seneviratne, S.I., Ward, P.J., Pitman, A., AghaKouchak, A., Bresch, D.N., Leonard, M., Wahl, T., Zhang, X., 2018. Future climate risk from compound events. Nat. Clim. Chang. 8, 469–477. https://doi.org/10.1038/s41558-018-0156-3.

Statistics, 2024. Statistical Bulletin of Haikou National Economic and Social Development in 2023. Available at: http://tjj.haikou.gov.cn/ (accessed 10 November 2024).